An aridity index-based formulation of streamflow components

Antonio Alves Meira Neto[1,2], Tirthankar Roy[3], Paulo Tarso Sanches de Oliveira[4], Peter A. Troch[2,3]

1. *Hydrology and Atmospheric Sciences, The University of Arizona, USA*
2. *Institute of Climate Studies, Federal University of Espírito Santo, Brazil*
3. *Civil and Environmental Engineering, University of Nebraska-Lincoln, USA*
4. *Hydrology and Water Resources, Federal University of Mato Grosso do Sul, Brazil*
5. *Biosphere 2, The University of Arizona, USA*

Corresponding author: **antoniomeira@gmail.com**

Key points

1. Aridity index (ϕ) formulations for the combined estimation of direct runoff, baseflow and total streamflow are presented.
2. The formulations include physical reasoning on streamflow components at ϕ reaching its limiting conditions.
3. The proposed formulations can reproduce water balance partitioning of the L'vovich (1979) framework at the mean annual timescale.

Abstract

Direct-runoff and baseflow are the two primary components of total streamflow and their accurate estimation is indispensable for a variety of hydrologic applications. While direct runoff is the quick response stemming from surface and shallow subsurface flow paths, and is often associated with floods, baseflow represents the groundwater contribution to streams and is crucial for environmental flow regulations, groundwater recharge, and water supply, among others. L'vovich (1979) proposed a two-step water balance where precipitation is divided into direct runoff and catchment wetting followed by the disaggregation of the latter into baseflow and evapotranspiration. Although arguably a better approach than the traditional Budyko framework, the physical controls of direct runoff and baseflow are still not fully understood. Here, we investigate the role of the aridity index (ratio between mean annual potential evapotranspiration and precipitation) in controlling the long-term (mean-annual) fluxes of direct runoff and baseflow. We present an analytical solution beginning with similar assumptions as proposed by Budyko (1974), leading to two complementary expressions for the two fluxes. The aridity index explained 83% and 91%, of variability in direct runoff and baseflow from 499 catchments within the continental US, and our formulations were able to reproduce the patterns of water balance proposed by L'vovich (1979) at the mean annual timescale. Our approach allows for the prediction of baseflow and direct runoff at ungauged basins and can be used to further understand how climate and landscape controls the terrestrial water balance at mean annual timescales.

Keywords

Long-term Fluxes, L'vovich Formulation, Budyko Formulation, Baseflow, Direct-runoff, Catchment Water Partitioning

1. Introduction

1.1. Background

Direct runoff (Q_D) and baseflow (Q_B) are the two main components of total streamflow (Q). Q_D represents the fast response of the catchment to rainfall, which is generated either by infiltration-excess (Horton, 1933) or saturation-excess (Dunne and Black, 1970) runoff. On the other hand, Q_B denotes the slow response of the catchment, which is the portion of water that did not leave the catchment as direct runoff or evapotranspiration, but contributed to the groundwater system (L'vovich, 1979; Ponce and Shetty, 1995a; Miller et al., 2016). Understanding the controls on these individual responses is of great importance to advance hydrologic sciences: For example, Q_D is associated with floods (Blöschl et al., 2019) and soil erosion (Morgan and Nearing, 2011), while Q_B is crucial for environmental flow regulation, groundwater recharge, and water supply (Miller et al., 2016; Graaf et al., 2019).

The need to provide freshwater for the growing populations combined with the effects of climate change has motivated studies on the prediction of global-scale groundwater recharge (Döll and Fiedler, 2008) and the assessment of climate change impacts on groundwater systems (Green et al., 2011; Taylor et al., 2012; Walvoord et al., 2016), more specifically, on groundwater recharge (Smerdon, 2017; Mohan et al., 2018). Catchment-scale formulations of baseflow can provide additional insights on those issues as baseflow can represent groundwater recharge at sufficiently long time-scales: the portion of water that is not lost as direct runoff or evaporation will eventually recharge a shallow aquifer and exit the catchment as baseflow. This simple yet practical approach was found to be useful in several studies on groundwater recharge estimation (Meyboom, 1961; Nathan and McMahon, 1990; Fröhlich et al., 1994; Wittenberg and Sivapalan., 1999; Walker et al., 2018).

While the estimation of direct runoff has a long tradition in hydrologic sciences, most notably with the curve number (SCS-CN) method (NRCS, 2004) for event-based direct runoff estimation, very few studies investigated the controls on the mean annual direct runoff ($\overline{Q_D}$), whereas the controls and mechanisms of baseflow generation are still not

fully understood. One of the earlier studies in which both Q_D and Q_B have been explicitly considered into a framework for annual water balance was conducted by L'vovich (1979), where the author classified these fluxes as "genetically distinct" responses of a catchment. In that study, the author observed a similar behavior between the annual expressions of precipitation and direct-runoff, and between catchment wetting (amount of precipitation not leaving through direct runoff) and baseflow. L'vovich (1979) noted that such patterns were consistent with geographic location but did not attribute physically meaningful parameters to account for the observed differences. This framework was not investigated any further until Ponce and Shetty (1995a, 1995b) developed a mathematical framework to account for the observed patterns. Although they could eventually reproduce the patterns found in L'vovich's (1979), a physical linkage between climatic and landscape properties and the assigned parameters was not attempted. More recently, Sivapalan et al (2011) investigated the L'vovich framework through the mathematical formulation of Ponce and Shetty (1995a) for a group of 431 catchments within the conterminous US and were able to shed light on the physical meaning of the assigned parameters by analyzing their spatial distributions across different climates. Their study, however, does not establish physical linkages between the Ponce and Shetty (1995a) model parameters and climatic and/or landscape properties. A similar approach, as in Sivapalan et al (2011), was followed by Gnann et al., (2019), who also used the Ponce and Shetty (1995a, 1995b) model to explain the baseflow dissimilarities between catchments within the U.S and the U.K.

The climatic controls on the mean-annual streamflow ($\bar{Q}$) have received much attention in the hydrologic literature, and its commonly explained through the Budyko framework (Budyko, 1979). In this framework, the climate is represented by the aridity index (ϕ), which is the ratio between mean-annual potential evapotranspiration ($\overline{PET}$) and mean-annual precipitation ($\bar{P}$). The Budyko framework has been widely used for global assessments of the impacts of climate change on streamflow through differentiation of the Budyko equation (or some parametric version of it) with respect to its controlling variables (Dooge et al., 1999; Arora, 2002; Renner et al., 2012; Roderick et al., 2014; Berghuijs et al., 2017) while also being used for prediction at ungauged sites (Blöschl et al., 2013). Additionally, several studies have used this framework to draw inferences on catchment behavior at mean annual timescales by analyzing how factors other than ϕ can explain

observed departures from observed data against the Budyko equation (Donohue et al., 2007; Berghuijs et al., 2014).

Wang and Wu (2013) have shown that the baseflow fraction (the ratio between baseflow and precipitation at the mean-annual scale i.e. $\overline{Q_B}/\bar{P}$) and runoff coefficient ($\bar{Q}/\bar{P}$) follow similar behaviors when plotted against ϕ for 185 perennial catchments located within the continental U.S. Wang and Wu (2013) derived an equation to express this relationship quantitatively, providing an interesting way to study the controls of climate on $\overline{Q_B}$. However, the equation presented in Wang and Wu (2013) have not been thoroughly analyzed for the limiting case of $\phi \to 0$, as it will be seen in **Section 1.4.** More recently, Gnann et al., (2019) conducted a study to understand whether ϕ can be used to predict the baseflow fraction. Their study was based on the analysis of several hundreds of catchments from the continental U.S and the U.K and their results suggest that ϕ alone cannot be used for such task. Following that, the authors parameterized the Ponce and Shetty (1995a) model to investigate the controls on baseflow generation within their group of catchments.

In this study, we discuss the role of ϕ on $\overline{Q_B}$ and $\overline{Q_B}$ over a wide range of ϕ and then propose an analytical derivation that leads to two expressions for the controls of ϕ on $\overline{Q_D}$ and $\overline{Q_B}$. We further investigate the ϕ-based formulations as potential solutions for the water balance framework proposed by L'vovich (1979) at the mean annual timescale. The paper is organized as follows. **Section 1.2** and **1.3** provide a revision of the Budyko (1974) and L'vovich (1979) frameworks, where we discuss in detail both frameworks and establish a common nomenclature. In **Section 1.4**, we present an approach for the analytical derivation of predictive equations for $\overline{Q_D}$ and $\overline{Q_B}$ based on the decomposition of $\bar{Q}$ into its complementary fluxes under similar assumptions as in Budyko (1974). This approach also provides a solution for the L'vovich (1979) framework at the mean-annual scale. **Section 2** presents the dataset and methods used in this study. Following that, in **Section 3**, we evaluate the proposed derivation to fit predictive equations for 499 catchments within the conterminous U.S. and test the predictive capacity of the derived equations for both $\overline{Q_D}$, $\overline{Q_B}$ and $\bar{Q}$ while also assessing their ability to reproduce the spatial (between-catchments) patterns arising from the two-step water-balance proposed by L'vovich (1979).

1.2. The Budyko Framework

Under the assumption of negligible changes in storage over sufficiently long timescales, the water balance can be written as the partitioning of $\bar{P}$ into $\bar{Q}$ and $\bar{E}$:

$$\bar{P} = \bar{Q} + \bar{E} \tag{1}$$

Several studies have been carried out in the past with a goal of understanding the overall controls on this simple partitioning. The water balance framework proposed by Budyko (1974) and others (Schreiber, 1904; Ol'dekop, 1911; Turc, 1954; Mezentsev, 1955; Pike, 1964) is still widely used and its success lies in the observation that the fraction of precipitation that becomes evaporation (evaporation fraction, $\bar{E}/\bar{P}$) is largely controlled by ϕ If we normalize the terms of **Equation 1** by $\bar{P}$ and assume this control to be translated into a functional relationship, we can write:

$$\frac{\bar{E}}{\bar{P}} = 1 - \frac{\bar{Q}}{\bar{P}} = f_E(\phi) \tag{2}$$

Where f_E is the function that relates $\bar{E}/\bar{P}$ to ϕ. When such relationship is defined, a simple formulation for the prediction of long-term streamflow can be derived as:

$$\bar{Q} = P \times \left(1 - f_E(\phi)\right) \tag{3}$$

In developing a functional form for $f_E(\phi)$, Budyko (1974) observed that the following conditions must be met:

$$\phi \to \infty \therefore \ \bar{E}/\bar{P} \to 1\,, and\ \bar{Q}/\bar{P} \to 0 \tag{4}$$

$$\phi \to 0 \therefore \ \bar{E}/\bar{P} \to 0\,, and\ \bar{Q}/\bar{P} \to 1$$

Several functional forms satisfying the above constraints have been proposed in the literature (Ol'Dekop, 1911, Turc, 1954; Mezentsev, 1955), the most common being the one proposed by Budyko (1974):

$$\bar{E}/\bar{P} = [\phi \times (1 - \exp\phi) \times \tanh\phi^{-1}]^{0.5} \tag{5}$$

Figure 1-A shows this formulation for $\bar{Q}/\bar{P}$.

1.3. The L'vovich Framework

In the framework proposed by L'vovich (1979), the annual water balance partitioning is taken as a two-step process. In the first step, the annual precipitation (p) is partitioned into annual direct runoff (q_D) and annual catchment wetting (ω):

$$p = q_D + \omega, \tag{6}$$

Whereas ω is further partitioned into annual baseflow (q_B) and annual evapotranspiration e:

$$\omega = q_B + e, \tag{7}$$

Equation 6 and **7** can be combined as:

$$p = q_D + q_B + e \tag{8}$$

Upon observing the distinct patterns between the individual components of the two-step water partitioning in catchments across different geographical locations, L'vovich (1979) developed relationships, as shown in **Figure 1-B** through **E**, where the blue lines represent the general shape of the curves in that study. It can be seen that ω and q_D respond differently to the increase in p: On one hand, ω increases almost linearly at low values of p, eventually reaching a maximum (**Figure 1-B)**. On the other hand, q_D is initially zero at the low values of p, and will only be observed when a threshold value of p is exceeded. After that, q_D increases rapidly with p (**Figure 1-D)**. A similar behavior can be found for the partitioning of ω between q_B and e in **Figure 1-C** and **E**.

1.4. Climate-based Formulations for Budyko and L'vovich Frameworks

From **Equation 2**, the runoff coefficient ($\bar{Q}/\bar{P}$) can be derived as:

$$f_R(\phi) = 1 - f_E(\phi) \tag{9}$$

By using **Equation 8** written in terms of mean-annual fluxes, the water balance can be written as:

$$\frac{\bar{Q}}{\bar{P}} = \frac{\overline{Q_D}}{\bar{P}} + \frac{\overline{Q_B}}{\bar{P}} \tag{10}$$

Combining **Equations 9** and **10** we get:

$$\frac{\overline{Q_D}}{\bar{P}} + \frac{\overline{Q_B}}{\bar{P}} = f_R(\phi) \tag{11}$$

which demonstrates the connection between the aridity index and the two complementary partitioning indices arising from the L'vovich (1979) formulation at the mean-annual timescale. If both left-hand terms can be written as a function of ϕ, we have:

$$f_R(\phi) = f_D(\phi) + f_B(\phi) \tag{13}$$

where:

$$\frac{\overline{Q_D}}{\bar{P}} = f_D(\phi) \tag{14}$$

$$\frac{\overline{Q_B}}{\bar{P}} = f_B(\phi) \tag{15}$$

Following the same reasoning as Budyko (1974), we can apply limiting conditions to the relationships in **Equation 14** and **15**. With values of ϕ approaching infinity, $\bar{Q}/\bar{P}$ will tend to zero, which leads to both $\overline{Q_D}/\bar{P}$ and $\overline{Q_B}/\bar{P}$ approaching zero as well:

$$with\ \phi \to \infty, \qquad \frac{\bar{Q}}{\bar{P}} = \frac{\overline{Q_D}}{\bar{P}} + \frac{\overline{Q_B}}{\bar{P}} \to 0 \tag{16}$$

$$thus, \qquad f_D \to 0\ ;\ f_B \to 0$$

As ϕ reaches zero, $\bar{Q}/\bar{P}$ will be one. In this way, some combination of $\overline{Q_D}/\bar{P}$ and $\overline{Q_B}/\bar{P}$ must occur such that their sum is equal to one, which also means that the maximum values of $\overline{Q_D}/\bar{P}$ and $\overline{Q_B}/\bar{P}$ can be derived from the limiting conditions:

$$with\ \ \phi \to 0, \qquad \frac{\bar{Q}}{\bar{P}} = \frac{\overline{Q_D}}{\bar{P}} + \frac{\overline{Q_B}}{\bar{P}} \to 1 \tag{17}$$

$$therefore, \qquad f_D \to \left[\frac{\overline{Q_D}}{\bar{P}}\right]_{max}$$

$$and, \qquad f_B \to \left[\frac{\overline{Q_B}}{\bar{P}}\right]_{max} = 1 - \left[\frac{\overline{Q_D}}{\bar{P}}\right]_{max}$$

If such relationships are established, one can re-write the variables from the L'vovich formulation as:

$$\overline{Q_D} = \bar{P}.f_D \tag{18}$$

$$\overline{W} = \bar{P} - \overline{Q_D} = \bar{P} - \bar{P}.f_D = \bar{P}.(1 - f_D) \tag{19}$$

$$\overline{Q_B} = \bar{P}.f_B \tag{20}$$

$$\bar{E} = \bar{P} - \overline{Q_B} - \overline{Q_D} = \bar{P}.(1 - f_D + f_B) \tag{21}$$

where $\overline{W}$ represents the mean-annual catchment wetting.

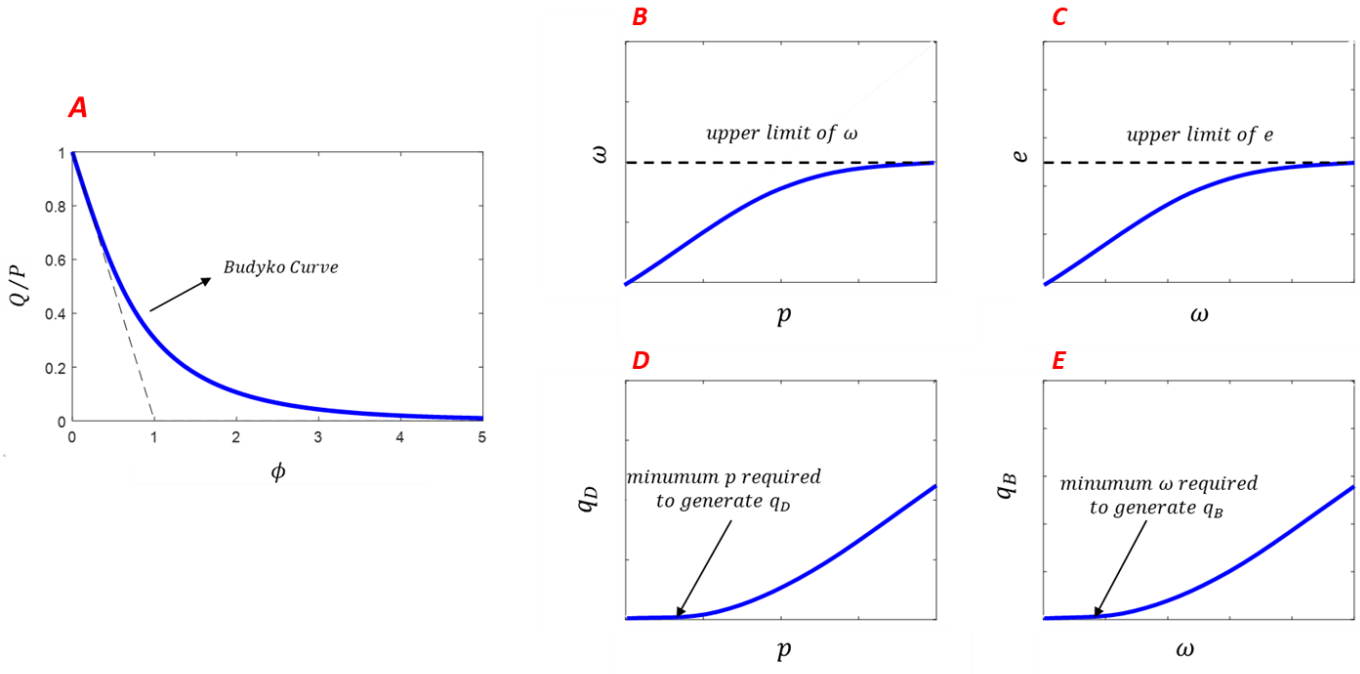

Figure 1. A- The Budyko framework for mean-annual water balance, where the aridity index (ϕ) appears to be the main control on the ratio between total streamflow and precipitation ($\overline{Q}/\overline{P}$) at the mean-annual scale. The blue line shows the empirical curve fitted by Budyko (1957). **B** - The L'vovich (1979) model for annual water balance, showing the first step, where p is partitioned into ω (B.1) and q_D (B.2), whereas in the second step, ω is partitioned into e (B.2) and q_B (B.4). The blue lines represent the general behavior observed at the annual scale.

2. Methods

2.1. Catchments and Hydrological Data

The catchments selected for this study are part of the CAMELS dataset (Addor et al., 2017), which is available online and contains daily time-series of streamflow and precipitation, among other variables. The meteorological variables used within the CAMELS dataset are described in Newman et al., (2015). The time period of analysis was 30 hydrologic years (October 1st through September 30st, between 1983 and 2013). We removed the catchments with more than 1% missing values of streamflow and negative mean annual evaporation ($\bar{E} < 0$). The resulting subset comprised data for 499 catchments (**Figure 2**).

Daily streamflow time-series were separated into daily values of direct-runoff and baseflow with a one-parameter, recursive low-pass filter (Lyne and Hollick, 1979). The filter parameter was set to 0.925 for all catchments to assure consistency. The filtering approach has been used in several recent studies (Sivapalan et al., 2011; Gnann et al. 2019). Finally, we calculated $\bar{Q}$, $\overline{Q_D}$, $\bar{W}$, $\overline{Q_B}$, and $\bar{E}$ using **Equation 1**, **6**, **7,** and **8**. Additionally, daily precipitation values where aggregated into mean annual $\bar{P}$ for each of the selected catchments.

2.2. Aridity Index Calculation

We used the Reference-crop Penman-Monteith formulation for calculating daily values of PET (in mm) as:

$$PET = \frac{0.408\Delta(Rn - G) + \gamma \frac{900}{T + 273} u(es - e)}{\Delta + \gamma(1 + 0.34u)} \quad (22)$$

Where Rn is the net radiation at the surface $(MJ.m^{-2}.day^{-1})$ is the heat flux into the subsurface in $(MJ.m^{-2}.day^{-1})$, e and e_S are respectively the actual and saturated vapor pressure $(kPa.K^{-1})$, u is the wind speed at 2 m $(m.s^{-1})$, T is the air temperature at 2 m (K), Δ is the slope of the relationship between saturation vapor pressure and temperature $(kPa.K^{-1})$ and γ is the psychrometric constant $(kPa.K^{-1})$. Rn was calculated as:

$$Rn = Rs(1 - \alpha) + Rnl \quad (23)$$

Where Rs is the incoming solar radiation $(MJ.m^{-2}.day^{-1})$, α is the albedo of the reference surface ($\alpha = 0.23$), and Rnl is the net longwave radiation $(MJ.m^{-2}.day^{-1})$. Briefly, we computed equations 22 and 23 based on the procedure described in Zotarelli et al., (2009). Daily Rs and u values were extracted for the CAMELS catchments from the gridMET dataset (Abatzoglou, 2013), whereas the other necessary variables where used where directly provided within the CAMELS dataset. Following that, we aggregated the PET into mean annual values and computed ϕ.

In our study, we chose to estimate PET rather than use the estimates provided with the CAMELS dataset, which are first presented in Newman et al., (2015). This was done since Newman et al., (2015) used a form of the Priestley and Taylor (REF) equation in which one of its variables was used as a calibrated parameter within a hydrologic model. The estimation of this parameter, therefore, will be largely affected by errors and uncertainties in model inputs, parameters, structures, among others. Furthermore, the PET estimates of Newman et al., (2015) are not reproducible, making the verification of our results impossible for other regions of the globe. We believe that a parsimonious representation of PET, and consequently ϕ, is crucial for our analysis, since the estimated value of ϕ determines the location of a catchment along the x-axis of the Budyko plot, which can potentially impact our results.

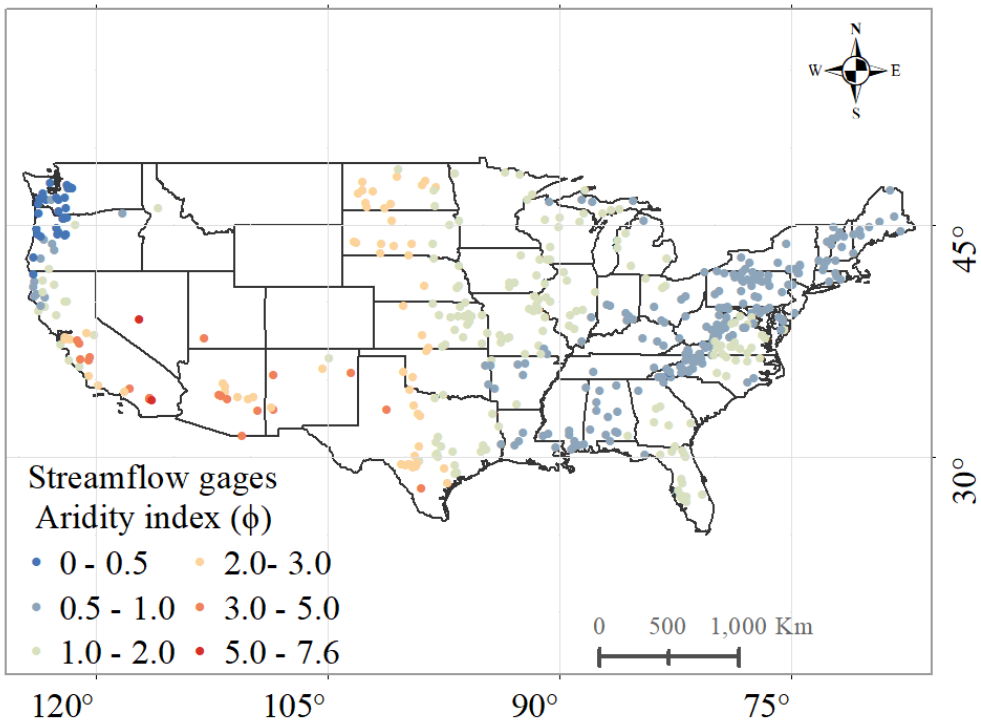

Figure 2 - Location of streamflow gages for the 499 catchments with complete records used in our study, color coded by the assigned value of ϕ.

3. Results

3.1. Analysis of Observed Mean-Annual L'vovich Water Balance Variables

Figure 3 shows the mean-annual components of the L'vovich (1979) water balance**.** We note a clear pattern of increment in both $\bar{W}$ and $\overline{Q_D}$ with $\bar{P}$ (subplots A and D), while the concavity of the relationships is similar to what can be seen in **Figure 1-B** through **E**. A threshold value for the initiation of $\overline{Q_D}$, as suggested by L'vovich (1979), is also observed in **Figure 1-B,** while the existence of a limiting upper value of $\bar{W}$ was not found for the selected CAMELS catchments.

The between-catchment patterns of the second partitioning are shown in **Figure 3-B** and **D.** We find an increasing trend in $\bar{E}$ with $\bar{W}$, but with higher variability. This trend, however, is not preserved for values of $\bar{W}$ around 1400 mm and higher. In fact, not only $\bar{E}$ is highly scattered around $\bar{W} \sim 1400\ mm$, it also seems to decrease, at least for its upper limit. The patterns of $\overline{Q_B}$ with $\bar{W}$ are, however, more consistent, with increasing values of $\bar{W}$ leading to an increase in $\overline{Q_B}$ in a similar fashion as in **Figure 1-E**. A threshold value for the initiation of $\overline{Q_B}$ can also be seen.

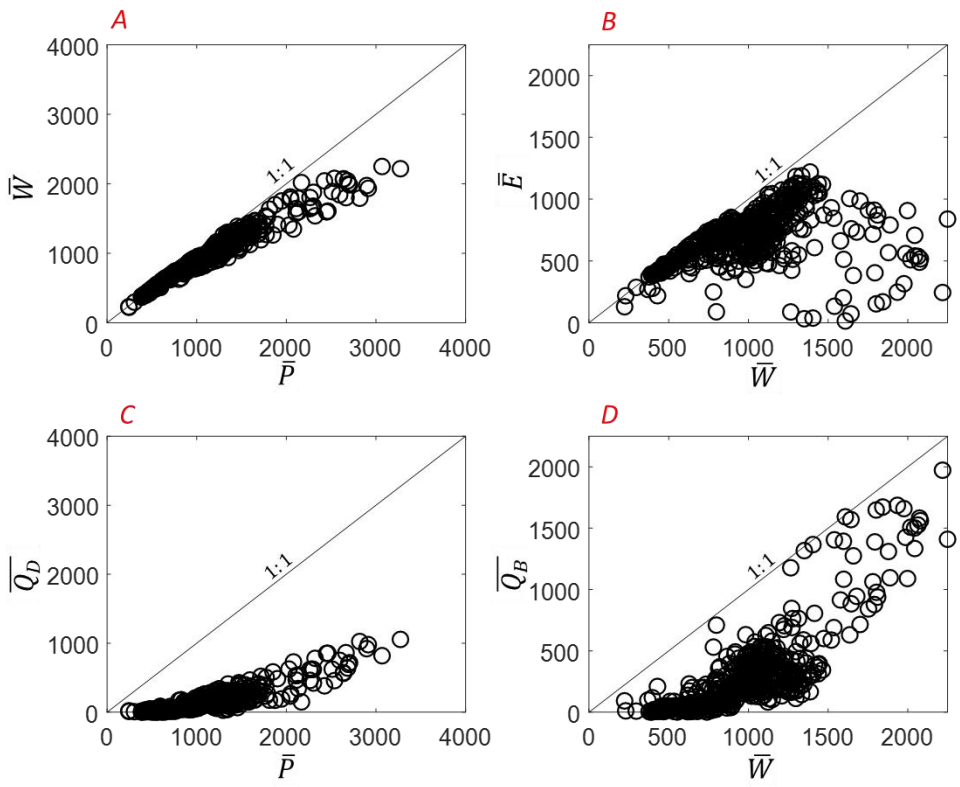

∗ *all axis in mm*

Figure 3 – Location of the selected CAMELS catchments (n=499) with respect to the L'vovich water balance, at the mean-annual time scale. While $\boldsymbol{P}$ appears to exert strong control on both $\overline{\boldsymbol{W}}$ and $\overline{\boldsymbol{Q_D}}$ (subplots A and C, respectively), much higher variability is present in the patterns between $\overline{\boldsymbol{W}}$ and $\overline{\boldsymbol{E}}$ (subplot B) and $\overline{\boldsymbol{W}}$ and $\overline{\boldsymbol{Q_B}}$ (subplot D). Interestingly, the suggested limits for $\overline{\boldsymbol{W}}$ and $\overline{\boldsymbol{E}}$ (Figure 1 B.1 and B.2) are not seen at the mean-annual scale. Note that $\boldsymbol{E}$ is maximum for a $\boldsymbol{W}$ value close to 1400 mm.

3.2. Functional forms of f_D and f_B

These observed patterns of $\overline{Q_D}/\overline{P}$ and $\overline{Q_B}/\overline{P}$ are shown in **Figure 4**, where a similarity in the patterns of both ratios as a function of ϕ is apparent. Additionally, a wide range of ϕ values is observed, ranging from 0.2 to 7.6. For simplicity, we used the functional form of an exponential decay to estimate f_D and f_B as:

$$f_D(\phi) = \exp\left(\phi^{\alpha} + \delta_D\right) \tag{24}$$

$$f_B(\phi) = \exp\left(\phi^b + \delta_B\right) \tag{25}$$

where a and b are shape parameters, while δ_D and δ_B are shifting coefficients necessary to satisfy conditions of **Equation 17**:

$$f_D(0) = \left[\frac{\overline{Q_D}}{\bar{P}}\right]_{max} \quad ; \quad f_B(0) = \left[\frac{\overline{Q_B}}{\bar{P}}\right]_{max} \tag{26}$$

Leading to:

$$\delta_D = \ln\left(\left[\frac{\overline{Q_D}}{\bar{P}}\right]_{max}\right) \quad ; \quad \delta_B = \ln\left(1 - \left[\frac{\overline{Q_D}}{\bar{P}}\right]_{max}\right) \tag{27}$$

We followed a manual procedure for fitting of the exponents through visual assessment of the resulting curves against observed values of **Figure 4**, while also computing the coefficient of determination (R^2) and fitting a regression line between observed and predicted fluxes $\overline{Q_D}$, $\overline{Q_B}$, and $\bar{Q}$ in order to assess the bias between predicted and observed values. After fitting the exponents, we assessed the robustness of the results by testing the resulting formulation on randomly sampled subsets having half of the sample size (n=249). We repeated the resampling and testing procedure 1000 times, recording the resulting R^2 of the predicted fluxes from each round to further compute its mean and coefficient of variation.

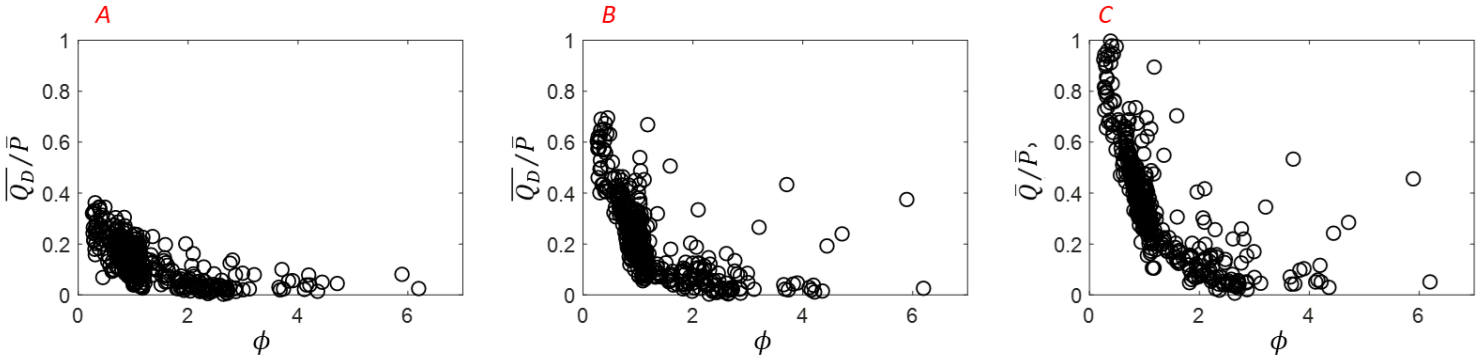

Figure 4 - Observed values of $\overline{Q_D}/\bar{P}$ (subplot A), $\overline{Q_B}/\bar{P}$ (subplot B), and $\bar{Q}/\bar{P}$ (subplot C) against ϕ for the selected subset of the CAMELS data-set (n=499). A similar pattern is observed among the curves, suggesting a similar functional form. It is worth noting that the limiting values of both $\overline{Q_D}/\bar{P}$ and $\overline{Q_B}/\bar{P}$ are evident in A and B for ϕ approaching 0.

3.3. Resulting Equations for f_D and f_B and their Predictive Performances

The fitting procedure described above allowed us to write the final functions as:

$$f_D(\phi) = \exp(\phi + \ln(0.36)) \quad (28)$$

$$f_B(\phi) = \exp(\phi^{1.6} + \ln(0.64)) \quad (29)$$

The fitted exponents for f_D and f_B are shown in the left column of **Table 1**, whereas **Figure 5** shows a plot of **Equations 28** and **29** against observed values (subplots A and B). Additionally, f_R as predicted by the Budyko (1974) through **Equation 5**, is also shown as a blue line in subplot C. It is clear from the figures that the suggested functional form was able to reproduce the observed patterns quite well and the resulting curve $f_R(\phi)$ follows a very similar trajectory as the Budyko curve, with some noticeable differences in horizontal position of the curve against the data. Such differences are somehow expected since our dataset was not the same as the one used in the original work of Budyko (1974). More importantly, it is not the objective of this work to provide an exact derivation of **Equation 5.**

The predictive capabilities of the derived equations can be seen at right column of **Table 1**, as the mean and coefficient of variation (C.V) of the R^2 from the resampling procedure described in **Section 3.2.** These results provide an insight on the role of ϕ as the main control of both $\overline{Q_D}$, $\bar{W}$, and $\overline{Q_B}$, as ϕ is able to explain 83%, 96%, and 91% of the between-catchment variability of these storage and flux terms. Moreover, the low variability in predictive performance as seen in low C.V values indicate a robust fit of the exponents of the selected functional form. **Figure 6** shows how the fitted curves performed against the observed values. A simple linear regression model (black dashed line) was fitted between observed and the predicted values discussed above and a 1:1 line (red dashed line) was added for reference. The slope of the regression line suggested a very low bias, around 1% for all fluxes.

We further explore the performance of the predicted relationships for the components of the L'vovich water balance at the mean-annual time-scale (**Figure 7**). The black circles represent the observed values for each catchment whereas the red circles are for the predicted values. Subplots A and C show a remarkable similarity between the observed and predicted variables of the first partitioning, confirming that the aridity index is able to explain great portion of the between-catchment variability, while also reproducing the trajectories of the progression between the competitions of $\overline{Q_D}$ and $\bar{W}$. The observed patterns for the second partitioning are shown in subplots B and D, from where similar conclusions can be drawn. The somehow scattered pattern in the relationship between W and E seemed to be well reproduced by the aridity index formulations (subplot B). It is worth noting that the decrease in $\bar{E}$ for $\bar{W}\sim$1400 mm and higher is also reproduced, reinforcing the hypothesis of such decrease to be a function of climate. Additionally, the patterns in $\overline{Q_B}$ as a function of $\bar{W}$ are also well reproduced both in magnitude of its variability as well as in the general shape of its increasing trajectory.

Table 1 – Results from the fitting procedure. Left: Estimates of the exponents (Equations 23 through 26). Right: Predictive capabilities of the fitted equation is presented as the mean and coefficient of variance (C.V) of the $\boldsymbol{R^2}$ based on 1000 randomly sampled subsets.

Parameter Estimates		***Predictive Capacity***		
Parameter	*Mean*	*Flux*	R^2 *mean*	R^2 *C.V*
$\left[\frac{\overline{Q_D}}{\bar{P}}\right]_{max}$	*0.36*	$\overline{Q_D}$	*0.83*	*2.6%*
a	*1.0*	$\bar{W}$	*0.96*	*0.4%*
b	*1.6*	$\overline{Q_B}$	*0.91*	*1.4%*
		$\bar{Q}$	*0.94*	*1.0%*

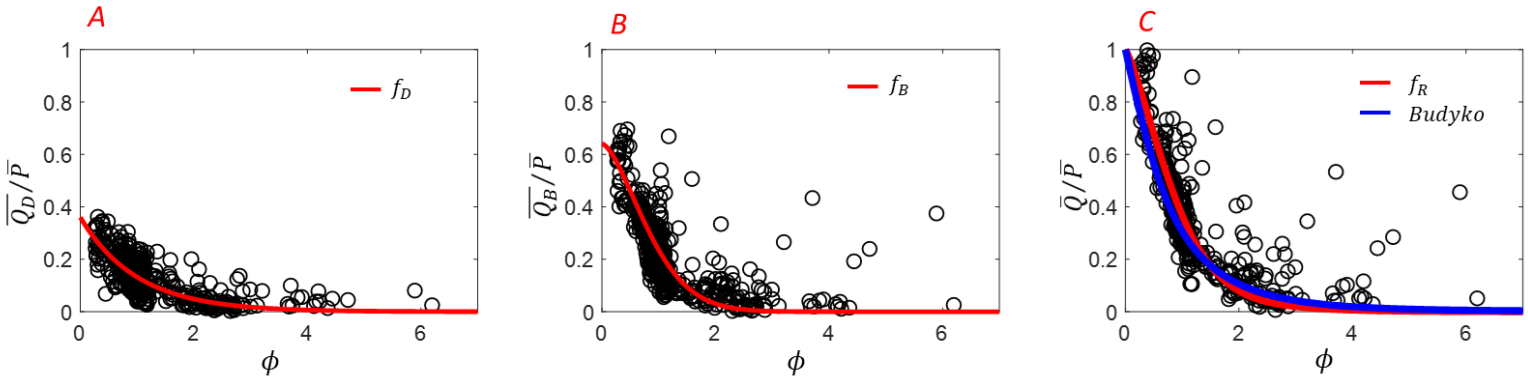

Figure 5. Observed values versus derived analytical equations for $\boldsymbol{f_D = \overline{Q_D}/\overline{P}}$ (subplot A), $\boldsymbol{f_B = \overline{Q_B}/\overline{P}}$ (subplot B), and $\boldsymbol{f = \overline{Q}/\overline{P}}$ (subplot C). The results of $\boldsymbol{\overline{Q}/\overline{P}}$ according to the equation proposed by Budyko (eqn. 5, blue line) are shown in subplot C for comparison.

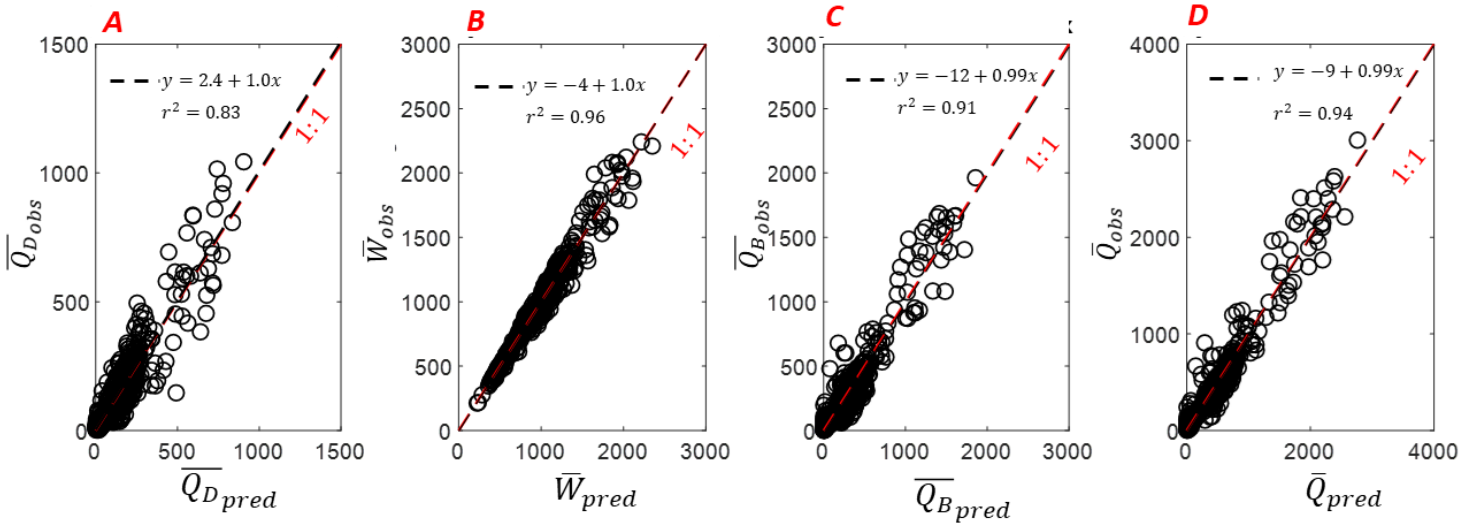

Figure 6. Observed versus predicted fluxes and explained variances for the 499 CAMELS catchments. An additional 1:1 line (dashed red line) is plotted for reference together with a linear regression (dashed black line) and regression coefficients. A: $\overline{Q_{D_{pred}}}$ calculated as in **Equation 18**. B: $\overline{W}_{pred}$ calculated as in **Equation 19** C: $\overline{Q_{B_{pred}}}$ calculated as in **Equation 20**. D: $\bar{Q}_{pred}$ calculated as in **Equation 21**.

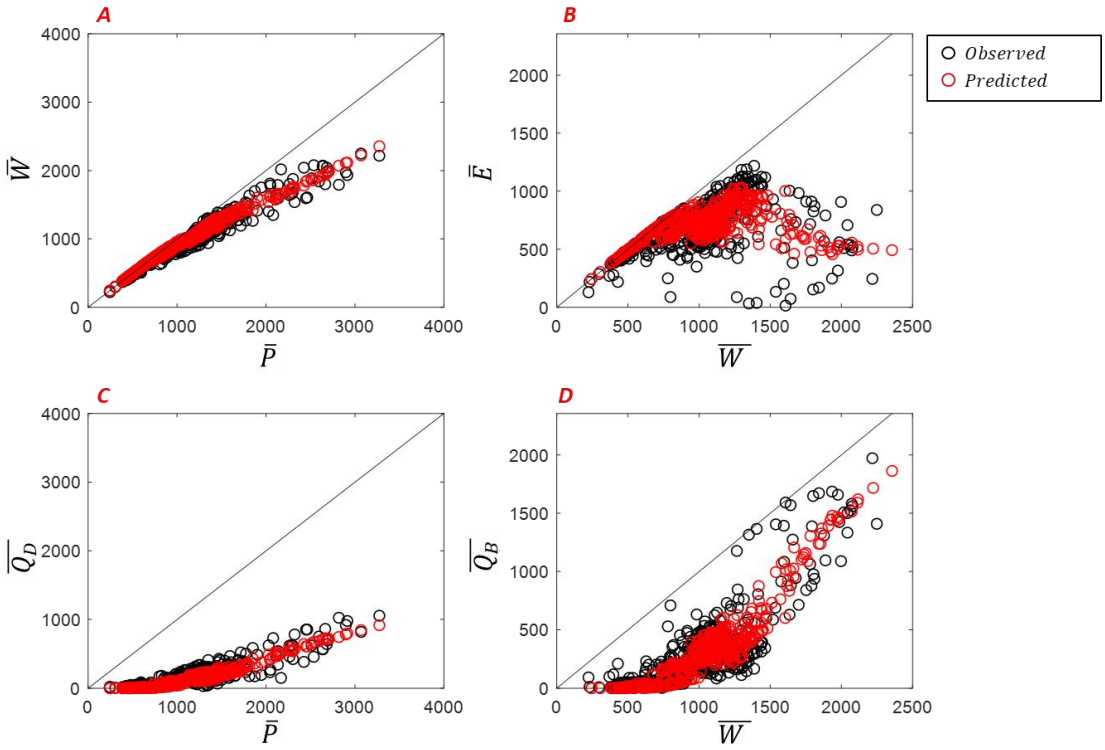

425

426 **Figure 7.** Comparison between the mean annual components of the L'vovich water balance
427 observed at the CAMELS catchments (black) and predicted by using equations 28 and 29
428 into equations 18 thorough 21. A good agreement can be seen in all subplots: Both patterns
429 of increase in $\overline{W}$ and $\overline{Q_D}$ with $\overline{P}$ are reproduced (subplots A and C), while similar patterns
430 of variability of $\overline{E}$ as a function of $\overline{W}$ were reproduced, including the decrease of $\overline{E}$ after
431 a threshold of $\overline{W}\sim$1400 mm. The increase in $\overline{Q_B}$ with $\overline{W}$ is also observed.

432
433
434
435

4. Discussion

Our findings highlight the role of climate on both direct-runoff and baseflow at the mean-annual timescale. The proposed approach differs from the one presented by Sivapalan et al., (2011) and Gnann et al., (2019), where a conceptual model for the partitioning was implemented, which lead to formulations requiring site-specific calibration. The importance of our results lies in the fact that there are very few catchment-scale formulations for the prediction of direct-runoff and baseflow at the mean annual timescale. Prediction of these fluxes at the catchment-scale is of paramount importance. Furthermore, our approach was able to encapsulate the impact of aridity index on both direct-runoff and baseflow contributions to the total streamflow, which has not been studied previously.

4.1. Role of ϕ on the Mean Annual $\overline{Q_D}$ and $\overline{Q_B}$

While enough evidence and mathematical frameworks have been thoroughly documented to explain and quantify different mechanisms in generating direct runoff at shorter timescales, to our knowledge, no study has shown how the long-term climate affects this hydrologic response. Moreover, our findings indicating that 84% of the variability of $\overline{Q_D}$ between the selected catchment is explained by aridity index alone can provide great insights on how event-based runoff mechanisms are propagated over longer timescales. Direct runoff is traditionally formulated at the event-scale as a function of storm-characteristics, land-surface properties and antecedent moisture conditions, such as in the Curve Number method (NRCS, 2004). Guswa et al., (2017) developed an approach based on the SCS-CN method with exponential distribution of rainfall depths to predict monthly and annual values of direct-runoff from 97 catchments in the conterminous US. However, their approach requires the estimation of the CN, which is a landscape-based parameter. While their method was able to predict with high accuracy the mean annual direct-runoff when using CN obtained on rainfall-streamflow analysis of the intended catchments, it performed poorly while using the readily available tabulated values of CN. We believe the aridity index to be an emerging descriptor of the interplay between event rainfall

(represented in $\bar{P}$) and antecedent moisture conditions, which is among other factors controlled by PET.

We have shown that the aridity index alone explains 91% of the variability of mean-annual baseflow. We confirmed the results shown in Wang and Wu (2013) regarding the similarity between f_R and f_B. However, their formulation provides a solution for f_B only and does not consider the limiting conditions for both baseflow and direct runoff coefficients at $\phi \rightarrow 0$. It is easy to observe in the equation from Wang and Wu (2013) that $\overline{Q_B}/\bar{P} \rightarrow \bar{Q}/\bar{P}$ at $\phi \rightarrow 0$, i.e. their solution assumes that at $\phi \rightarrow 0$, all rain becomes baseflow and no direct runoff is produced, which does corroborate with the findings from this study (see **Figure 4**-A).

Our results contradict the findings of Gnann et al., (2019), whose conclusion was that "there is no single baseflow Budyko curve, (…) baseflow fraction cannot be modelled as a function of an aridity index alone". Their main argument came from the observation that the baseflow coefficient ($\overline{Q_B}/\bar{P}$) "*did not always increase with decreasing* ϕ" after observing the behavior of a small subset of catchments with very low values of ϕ ($\phi \leq 0.2$, see *Figures 1B* and *Figure 10* of the referred study) located within the U.K. subgroup, in which catchments demonstrated a decrease in $\overline{Q_B}/\bar{P}$ with the decrease in ϕ. Two considerations regarding our study and Gnann et al., (2019) are made here. *First*, as suggested here, $\overline{Q_B}/\bar{P}$ will not always increase with decreasing ϕ since a maximum value of $[\overline{Q_B}/\bar{P}]_{max}$ should exist at the limiting case of $\phi \rightarrow 0$. As previously explained, if $\overline{Q_B}/\bar{P}$ is allowed to increase indefinitely for $\phi \rightarrow 0$, $\overline{Q_D}/\bar{P}$ would reach zero, meaning that in extremely humid climates all rainfall becomes baseflow and no direct-runoff is produced. Even though the catchments within our study do not fall under such low values of aridity index, with our lowest ϕ being equal to 0.25, the observed trends in both $\overline{Q_D}/\bar{P}$ and $\overline{Q_B}/\bar{P}$ with decreasing ϕ suggest the existence of such limiting conditions. *Second*, upon visual inspection of *Figure 1b* and *Figure 10* of that study, we estimate that a subset of approximately 10 catchments with $\phi \sim 0.2$ somehow does not follow the increasing trend with decreasing ϕ but that does not visually confirm a decreasing trend in $\overline{Q_B}/\bar{P}$ with ϕ, as argued by the authors. Considering the small sample size within such low range of values of ϕ with the addition of what has been shown in this study, that pattern can also be

interpreted as values of $\overline{Q_B}/\bar{P}$ reaching a plateau around a minimum value, or can be even interpreted as outliers. It is worth noting that the overall location of the U.K catchments within the $\overline{Q_B}/\bar{P}$ versus ϕ space in that study (triangles in *Figure 1b* and *Figure 10* of the referred study) suggest a very different behavior for that subgroup regardless of ϕ. An additional reason to further the discussion on the positioning of catchments within the $\overline{Q_B}/\bar{P}$ versus ϕ space in that study is the estimation of ϕ. The PET used for the U.S subset of their study were taken from Newmann et al., (2015), which are not solely based on observations of meteorological variables (see **Section 2.2**), whereas PET for their U.K subset were taken from different dataset (Robinson et al., 2016), and computed based on the FAO-Penman-Monteith (Allen et al., 1998) method. It is our opinion that the use of a single PET estimator, computed with a common set of inputs should be preferred when assessing differences in catchment behavior across datasets and varying ranges of ϕ.

We believe that behavior of $\overline{Q_B}/\bar{P}$ over very low values of ϕ is still uncertain and should be further investigated using more extensive datasets with a larger sample size around very low values of ϕ. Despite of that, the results shown here are clearly encouraging for the assessment of the role of climate on $\overline{Q_B}$ and $\overline{Q_D}$ over wide range of climatic regions, represented by the range of ϕ used in the derivation of the formulations of this study.

4.2. Controls of L'vovich Water Balance Formulation

While other studies have so far used the modelling framework of Ponce and Shetty (1995) (Sivapalan et al., 2011, and Gnann et al., 2019), the relationships from **Equation 18** through **21** were able to reproduce the overall patterns of partitioning and are based on semi-empirical relationships, without the need for calibration. Even though our analysis was performed at the mean-annual scale, it provides strong evidence for using the aridity index in interannual formulations of the water balance according to the L'vovich framework, as proposed in Sivapalan et al., (2011).

4.3. Broader Implications of the Proposed Method

Continental and global scale assessments of the impacts of climate change based on catchment-scale formulations of the water balance have a long tradition in hydrology. Most approaches have used the Budyko framework to assess the sensitivity of changes in ϕ or its individual components on $\bar{Q}$ (Dooge et al., 1999; Arora, 2002; Renner et al., 2012; Roderick et al., 2014; Berghuijs et al., 2017). These studies apply differentiation techniques to either the Budyko equation or some other parametric version of it to derive equations relating the effect of changes in aridity index or its separate components (Berghuijs et al., 2017) on total streamflow. It stands to reason that our proposed approach can undergo similar procedures, yielding assessments of the effects of climate change on $\overline{Q_D}$ and $\overline{Q_B}$. This might prove valuable for studies of the effects of climate on groundwater resources, as it has been previously shown in **Section 1**.

Another interesting venue for research is the investigation of other controlling factors on $\overline{Q_B}/\bar{P}$ and $\overline{Q_D}/\bar{P}$ at the mean-annual scale. Several studies that attempted to quantify departures from the Budyko curve by use of additional landscape and other climatic factors yielded invaluable insight on how such factors affect the long-term water balance (Donohue et al., 2007; Berguijs et al., 2014), while also improving the predictive capacity of $\overline{Q_D}$ and $\overline{Q_B}$ (Xu et al., 2013; Zhang et al., 2015). A similar procedure can be extended to the formulations presented here to further investigate the controls on baseflow and direct-runoff coefficient. We could start by asking how the already understood climatic and landscape features that are known to provide further insight into the controls on $\bar{Q}$ are translated into the control of its complementary components $\overline{Q_D}$ and $\overline{Q_B}$. Finally, our proposed approach may be used as a tool for the prediction of streamflow in ungauged basins as it uses easy-to-obtain variables and do not rely on specific site calibration.

6. Conclusion

The understanding and prediction of the water-balance beyond its traditional form which considers the total streamflow as its single response can yield invaluable insight needed for different hydrologic applications. While the two-step water balance formulation proposed by L'vovich (1979) appears as a promising venue for approaching this task, the need for the understanding of its underlying climatic and landscape controls has not yet allowed for the development of robust predictive tools.

We have provided a derivation of analytical expressions of the control of ϕ on both $\overline{Q_D}$ and $\overline{Q_B}$. The formulations presented here were able to explain most of the mean-annual (between catchment) variabilities of $\overline{Q_D}$, $\overline{Q_B}$ and $\bar{Q}$ and be valid predictive tools for those fluxes. Additionally, our solution was able to reproduce the observed patterns between the components of the L'vovich (1979) water balance at the mean annual timescale, and is based on the derivation of two complementary curves that when combined provide a solution for the $\bar{Q}$ that is similar to the widely known Budyko (1974) formulation. While further investigations for assessing the validity of the ϕ-based expressions when dealing with catchments with ϕ values lower than the observed here, the large sample size (n=499) and wide range of aridity indices (from $0.2 < \phi < 7.7$) of study are encouraging for the use of our method for regions beyond our study area.

Finally, we believe our method provides an extension for the assessments on how factors other than ϕ control the mean-annual runoff, this time allowing for the assessment of such factors on $\overline{Q_D}$ and $\overline{Q_B}$ and can also be used for estimating sensitivities of both components to changes in climate.

ACKNOWLEDGMENTS

Antonio A. M. N. would like to acknowledge the financial support received by the Brazilian Ministry of Education through the Brazilian Scientific Mobility Program from CAPES Foundation (finance Code 001). Paulo T. S. O. was supported by the Brazilian National Council for Scientific and Technological Development (CNPq) (grants 441289/2017-7 and 306830/2017-5) and the CAPES Print program. The CAMELS dataset is available from https://ncar.github.io/hydrology/datasets/CAMELS_attributes. The gridMET data can be downloaded at https://www.northwestknowledge.net/metdata/data/ . The final mean annual variables used here are accessible through https://figshare.com/articles/Shared_xlsx/11592015

REFERENCES

Abatzoglou, J. (2013, 1). Development of gridded surface meteorological data for ecological applications and modelling. *International Journal of Climatology*, *33*(1), 121-131.

Addor, N., Newman, A., Mizukami, N., & Clark, M. (2017). The CAMELS data set: Catchment attributes and meteorology for large-sample studies. *Hydrology and Earth System Sciences, 21*(10), 5293-5313.

Arora, V. (2002). The use of the aridity index to assess climate change effect on annual runoff. *Journal of Hydrology*, *265*(1-4), 164-177.

Budyko, M. I. (1974). Climate and life (508 pp.). New York, NY: Academic Press.

Blöschl, G., Sivapalan, M., Wagener, T., Viglione, A., & Savenije, H. (Eds.). (2013). Runoff Prediction in Ungauged Basins: Synthesis across Processes, Places and Scales. Cambridge: Cambridge University Press. doi:10.1017/CBO9781139235761

Blöschl, G., Hall, J., Viglione, A. *et al.* Changing climate both increases and decreases European river floods. *Nature* **573,** 108–111 (2019) doi:10.1038/s41586-019-1495-6

Berghuijs, W., Larsen, J., van Emmerik, T., & Woods, R. (2017). A Global Assessment of Runoff Sensitivity to Changes in Precipitation, Potential Evaporation, and Other Factors. *Water Resources Research, 53*(10), 8475-8486.

Döll, P., & Fiedler, K. (2008). *Hydrology and Earth System Sciences Global-scale modeling of groundwater recharge.*

Donohue, R., Roderick, M., & Mcvicar, T. (2007). *Hydrology and Earth System Sciences On the importance of including vegetation dynamics in Budyko's hydrological model.*

Dooge, J., Bruen, M., & Parmentier, B. (1999). A simple model for estimating the sensitivity of runoff to long-term changes in precipitation without a change in vegetation. *Advances in Water Resources*, *23*, 153-163.

Dunne, T., & Black, R. (1970). Partial Area Contribution to Storm Runoff in a Small New England. *Water Resources Research, 6*(5), 1296-1311.

Fröhlich, K., Frôhlich, W., & Wittenberg, H. (1993). *FRIEND: Flow Regimes from International Experimental and Network Data.* IAHS Publ.

Gnann, S., Woods, R., & Howden, N. (2019, 4 1). Is There a Baseflow Budyko Curve? *Water Resources Research, 55*(4), 2838-2855.

Graaf, I.E.M., Gleeson, T., (Rens) van Beek, L.P.H. et al. Environmental flow limits to global groundwater pumping. Nature 574, 90–94 (2019) doi:10.1038/s41586-019-1594-4

Green, T., Taniguchi, M., Kooi, H., Gurdak, J., Allen, D., Hiscock, K., . . . Aureli, A. (2011). Beneath the surface of global change: Impacts of climate change on groundwater. *Journal of Hydrology, 405(3-4)*, 532-560.

Guswa, A., Hamel, P., & Meyer, K. (2018). Curve number approach to estimate monthly and annual direct runoff. *Journal of Hydrologic Engineering, 23*(2).

Hartmann, A., Gleeson, T., Wada, Y., & Wagener, T. (2017). Enhanced groundwater recharge rates and altered recharge sensitivity to climate variability through subsurface heterogeneity. *Proceedings of the National Academy of Sciences of the United States of America*, *114*(11), 2842-2847.

Horton, R. E. (1933), The Role of infiltration in the hydrologic cycle, Eos Trans. AGU, 14(1), 446– 460, doi:10.1029/TR014i001p00446.

Lyne, V. D., and M. Hollick (1979), Stochastic time-variable rainfall runoff modelling, in *Hydrology and Water Resources Symposium*, pp. 82–92.

L'vovich, M. I. (1979), World Water Resources and Their Future, translated from Russian by R. L. Nace, 415 pp., AGU, Washington, D. C

649
650 Walvoord, M. (2016). Implications of projected climate change for groundwater recharge
651 in the western United States. *Journal of Hydrology, 534*, 124-138. Elsevier B.V.

652 Mezentsev, V. S. (1955), More on the calculation of average total evaporation, Meteorol.
653 Gidrol., 5, 24–26
654
655 Meyboom, P. (1961), Estimating ground-water recharge from stream hydrographs, *J.*
656 *Geophys. Res.*, 66(4), 1203– 1214, doi:10.1029/JZ066i004p01203.

657 Miller, M., Buto, S., Susong, D., & Rumsey, C. (2016). The importance of base flow in
658 sustaining surface water flow in the Upper Colorado River Basin. *Water*
659 *Resources Research, 52*(5), 3547-3562.

660 Mohan, C., Western, A., Wei, Y., & Saft, M. (2018). Predicting groundwater recharge for
661 varying land cover and climate conditions-a global meta-study. *Hydrology and*
662 *Earth System Sciences, 22*(5), 2689-2703.

663 Morgan, R. P. C.; Nearing, M. A. (Eds.), (2011). Handbook of erosion modeling. West
664 Sussex: Wiley-Blackwell, 2011.
665
666 Nathan, R. J., and McMahon, T. A. (1990), Evaluation of automated techniques for base
667 flow and recession analyses, *Water Resources Resear,ch* 26(7), 1465– 1473,
668 doi:10.1029/WR026i007p01465.
669
670 Newman, A., Clark, M., Sampson, K., Wood, A., Hay, L., Bock, A., . . . Duan, Q. (2015).
671 Development of a large-sample watershed-scale hydrometeorological data set for
672 the contiguous USA: Data set characteristics and assessment of regional
673 variability in hydrologic model performance. *Hydrology and Earth System*
674 *Sciences, 19*(1), 209-223.

675 NRCS (Natural Resources Conservation Service). (2004). "Estimation of direct runoff
676 from storm rainfall." ⟨http://www.wcc.nrcs.usda.gov/ftpref
677 /wntsc/H&H/NEHhydrology/ch10.pdf⟩
678
679 Ol'dekop, E. M. (1911), On evaporation from the surface of river basins, Trans.
680 Meteorol. Obs. Univ. Tartu, 4, 200.
681
682 Pike, J. G. (1964), The estimation of annual runoff from meteorological data in a tropical
683 climate, J. Hydrol., 12, 2116–2123.
684
685 Ponce, V., & Shetty, A. (1995a). A conceptual model of catchment water balance: 1.
686 Formulation and calibration. *Journal of Hydrology, 173*, 27-40.

687 Ponce, V., & Shetty, A. (1995b). A conceptual model of catchment water balance: 2.
688 Application to runoff and baseflow modeling. *Journal of Hydrology, 173*, 41-50.

689

690 Priestley, C., & Taylor, R. (1971). On the Assessment of Surface Heat Flux and
691 Evaporation Using Large-Scale Parameters. *Monthly Weather Review, 100*(2), 81-
692 92.

693

694 Renner, M., Seppelt, R., & Bernhofer, C. (2012). Evaluation of water-energy balance
695 frameworks to predict the sensitivity of streamflow to climate change. *Hydrology*
696 *and Earth System Sciences, 16*(5), 1419-1433.

697 Robinson, E., E. Blyth, D. Clark, E. Comyn-Platt, J. Finch, and A. Rudd (2016),
698 Climate hydrology and ecology research support system potential evapotran-
699 spiration dataset for Great Britain (1961-2015) [CHESS-PE]
700
701 Roderick, M., Sun, F., Lim, W., & Farquhar, G. (2014). A general framework for
702 understanding the response of the water cycle to global warming over land and
703 ocean. *Hydrology and Earth System Sciences, 18*(5), 1575-1589.

704 Schreiber, P. (1904), Ueber die Beziehungen zwischen dem Niederschlag und der
705 Wasserfvhrung der flvsse in Mitteleuropa, Z. Meteorol., 21, 441–452
706
707 Sivapalan, M., Yaeger, M., Harman, C., Xu, X., & Troch, P. (2011). Functional model of
708 water balance variability at the catchment scale: 1. Evidence of hydrologic
709 similarity and space-time symmetry. *Water Resources Research, 47*(2).

710 Smerdon, B. (2017). A synopsis of climate change effects on groundwater recharge.
711 *Journal of Hydrology, 555,* 125-128. Elsevier B.V.

712 Taylor, R., Scanlon, B., Döll, P., Rodell, M., Van Beek, R., Wada, Y., . . . Treidel, H.
713 (2013). Ground water and climate change. *Nature Climate Change, 3(4),* 322-329.

714 Turc, L. (1954), Le bilan d'eau des sols: Relation entre les precipitations, l'evaporation et
715 l'ecoulement, Ann. Agron. Serie A, 5, 491–595.
716 Walker, D., Parkin, G., Schmitter, P., Gowing, J., Tilahun, S., Haile, A., & Yimam, A.
717 (2019). Insights From a Multi-Method Recharge Estimation Comparison Study.
718 *Groundwater, 57*(2), 245-258.

719 Wang, D., & Wu, L. (2013). Similarity of climate control on base flow and perennial
720 stream density in the Budyko framework. *Hydrology and Earth System Sciences,*
721 *17*(1), 315-324.

722 Wittenberg, H., & Sivapalan, M. (1999). Watershed groundwater balance estimation
723 using streamflow recession analysis and baseflow separation. *Journal of*
724 *Hydrology, 219,* 20-33.

725 Xu, X., Liu, W., Scanlon, B. R., Zhang, L., and Pan, M. (2013), Local and global factors
726 controlling water-energy balances within the Budyko framework, *Geophys. Res.*
727 *Lett.*, 40, 6123– 6129, doi:10.1002/2013GL058324.
728

729 Zhang, D., Cong, Z., Ni, G., Yang, D., & Hu, S. (2015). Effects of snow ratio on annual
730 runoff within the Budyko framework. *Hydrology and Earth System Sciences*,
731 *19*(4), 1977-1992.

732 Zomlot, Z., Verbeiren, B., Huysmans, M., & Batelaan, O. (2015). Spatial distribution of
733 groundwater recharge and base flow: Assessment of controlling factors. *Journal*
734 *of Hydrology: Regional Studies*, *4*, 349-368.

735 Zotarelli, L., Dukes, M. D., Romero, C. C., Migliaccio, K. W., and
736 Morgan, K. T. (2009). Step by step calculation of the Penman-Monteith
737 Evapotranspiration (FAO-56 Method). University of Florida Extension, AE459, available
738 at: http://edis.ifas.ufl.edu
739